Tensile Constitutive Behaviors of FR mortars and HPFRCs

V. Savino[a], L. Lanzoni[b,c,], A.M. Tarantino[c], M. Viviani[a]

[a]*HEIG-VD - Haute Ecole d'Ingénierie et de Gestion du Canton de Vaud, Route de Cheseaux 1, CH-1401 Yverdon*
[b]*DESD - Dipartimento di Economia, Scienze e Diritto, University of San Marino, Salita alla Rocca 44, Republic of San Marino, 47890 San Marino*
[c]*DIEF-Department of Engineering "Enzo Ferrari", University of Modena and Reggio Emilia, 41125 Modena, Italy*

Abstract

Fiber reinforced mortars (FRMs) and high performance fiber reinforced concretes (HPFRCs) are today widely used as repair and strengthening composites for existing structures, with particular reference to bridges and other concrete structures. Once a strengthening material is available for the market, there is the need of quickly and inexpensively testing its physical characteristics to ensure engineers that the product meets the designer's requirements. Such testing methods, although simple, must be able to correctly characterize the ductility, the tensile strength, the flexural strength as well as to establish a correlation between such parameters. This paper deals with the characterization of the mechanical properties and the ductility indexes of three commercial FRCs. The study focuses on the correlations between the ductility and both the direct and indirect tensile strengths. The obtained experimental data were compared with those provided by a model based on the "Composite Material Theory" (CMT), showing good agreement.

Keywords: Metal-matrix composites; Mechanical properties; Damage mechanics; Mechanical testing

Email address: luca.lanzoni@unimo.it (L. Lanzoni)

1. Introduction

The technology of steel fiber reinforced concrete (SFRC) has much evolved in the past years thanks to a great number of researches performed both on the fiber-based materials [6, 13, 27, 29, 15, 32, 26, 28, 39] and on the applications [16, 1, 3, 23, 2]. New shapes and types of steels have been developed to improve the fibers and, in turn, the SFRC performances[4, 5, 12, 31][1]. The mixing procedures of SFRC have been shortened and simplified over the years. SFRC is today largely used to repair and strengthen existing structures (e.g. bridge decks, piers, etc.)[2]. When SFRCs are used as repair and strengthening materials, their mechanical behavior must be known a priori by the designer. The success of the SFRC has promoted the development of a number of commercial products that nowadays are commercially available and produced on large scale and according to precise technical data sheets. The mechanical performances of these commercial FRCs are affected by many parameters, with particular reference to the type of fibers, fibers dosages, geometry of tested specimens, fibers aspect ratio and the test methods also [14, 38, 25, 11, 10, 30]. Laboratory tests characterizing certain properties of SFRC (such as tensile strength, ductility and flexural strengths) are often time consuming and expensive. These characterization procedures are therefore ill-adapted to the need of a rapid and cheap performances control and validation that are usually required by the designers. To aid the practitioners and simplify the procedures, some technical guidelines have been developed and recently adopted in codes [33, 40, 41, 36, 37, 42, 43, 44, 45, 46, 47].

This paper deals with the mechanical characterization of three different SFRCs, two of which are UHPFRCs. The experimental tests have been made according to standard protocols in order to assess the compressive strength, direct tensile strength and flexural strength of the composites. In particular, compressive strength tests on cubic specimens, direct tensile tests on dog-bone specimens and four-point bending flexural tests, performed both on notched and un-notched prismatic specimens, were carried out. The behavior in terms of ductility was assessed accordingly.

The paper is organized as follows. A description about the procedures used to perform the investigation is provided in Section 2. In particular, in

[1]Recent studies about FRCs based on synthetic fibers can be found in [17, 24].

[2]An important issue concerning the mechanical interaction in time between the hosting structure and the reinforcemet is addressed in [8, 7, 9].

such a Section the experimental tests are described in some detail. Information about the concrete mixtures tested are also given in this Section. The main results provided by the experimental tests are reported and discussed in Section 3. Finally, conclusions are drawn in Section 4.

2. Materials and methods

In the present work the mechanical behavior of three different types of commercial FRCs (termed hereinafter “A”, “B” and “C”), are investigated through a standard procedure. For each type of mortar the producer prescribes in detail the following items[3]:

- Dosages of admixtures (inerts, water/cement ratio, plasticizers, accelerators, etc.);
- Quantity and type of steel fibers (hooked or straight, aspect ratio, etc.);
- Mixing, flowing and curing procedures.

The mix design for getting 1 m^3 of each mortar under testing is shown in Table 1. The solid part (binders and granular skeleton) of each mortar is different even if all of them were named “premix” by the producers. In fact, the producers supply the premix in sacks or big-bags that have to be used as a unit, i.e. a sack cannot be partially used.

	kg in 1 m^3 of composite		
material	A (HPC)	B (UHPC)	C(UHPC)
Premix	2226	2296	1970
Superplasticizer	22.3	43.13	39
Accelerator	-	10	-
Water	231	184	195
Hooked steel fibers 30/0.35 mm	130 (1.7 %)	-	-
Straight steel fibers 20/0.3 mm	-	195 (2.5 %)	-
Straight steel fibers 13/0.175 mm	-	-	296 (3.8 %)

Table 1: Mix design for the SFRCs under testing.

A premix usually contains cement, sands and pozzolans. The companies producing these mortars do not provide the composition of the premix and

[3]A recent study about a polymer-based mortar for retrofitting is performed in [20].

the nature of the compounds and chemicals. Each premix comes with a superplasticizer used to obtain the target water/cement ratio (that can be as low as 0.2). The superplasticizer is used at high dosage to increase the strength, enhance the durability and give high workability [48]. In the "B" mortar the manufacturers advise to add a set and hardening accelerator to shorten the dormant period and to speed up the hydration process. The type of fibers used for these concretes is usually chosen according to the target application.

Figure 1: Steel fibers used in the mortars: a) Hooked fibers 30/0.35 mm; b) Straight fibers 20/0.3 mm; c) Straight fibers 13/0.175 mm.

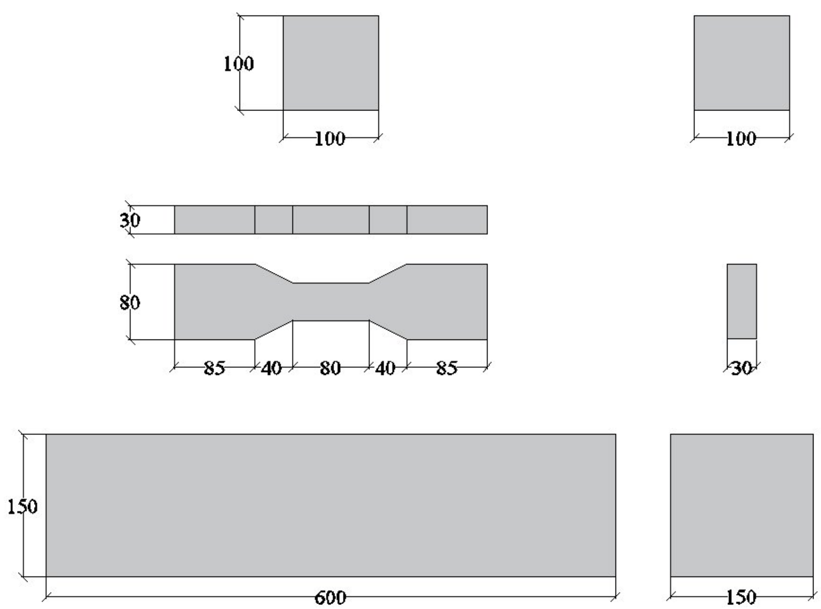

Figure 2: Specimen dimensions.

For structural applications steel fibers are usually preferred (see Fig. 1). Mixing HPC and UHPC requires the use of high intensity mixers. In this study a 1.5 kW high shear Zyklos rotating pan mixer was used to manufacture standard specimens to test tensile, flexural and compressive strengths. The types of tested specimens and their dimensions are shown in Fig. 2.

Compressive strength test on cubic specimens, direct tensile test on dog-bone specimens and four-point bending flexural tests, both on notched and un-notched prismatic specimens, were carried out. Standard tests configurations are shown in Fig. 3.

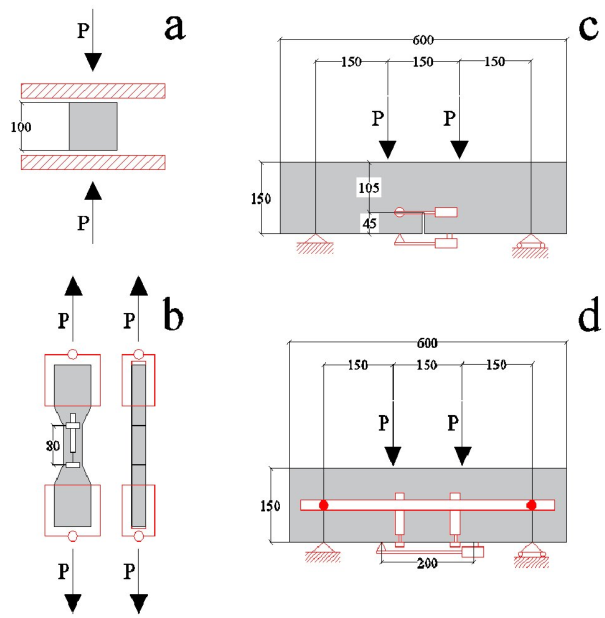

Figure 3: a) Compression test on cubic specimen; b) Direct tensile test on dog-bone specimen; c) Four-point bending test on notched beam specimen; d) Four-point bending test on un-notched beam specimen.

2.1. Compression tests

A compression machine Perrier type 138-5000 kN, as shown in Fig. 4(a), was used for the compression tests according to [49, 50, 51]. The loading speed of the compression machine was set to 6 kN/sec.

2.2. Direct tensile test

A machine Walter Bai type LVF-200 kN was used for the direct tensile test on dog-bone specimens. The rate of the axial elongation was set equal

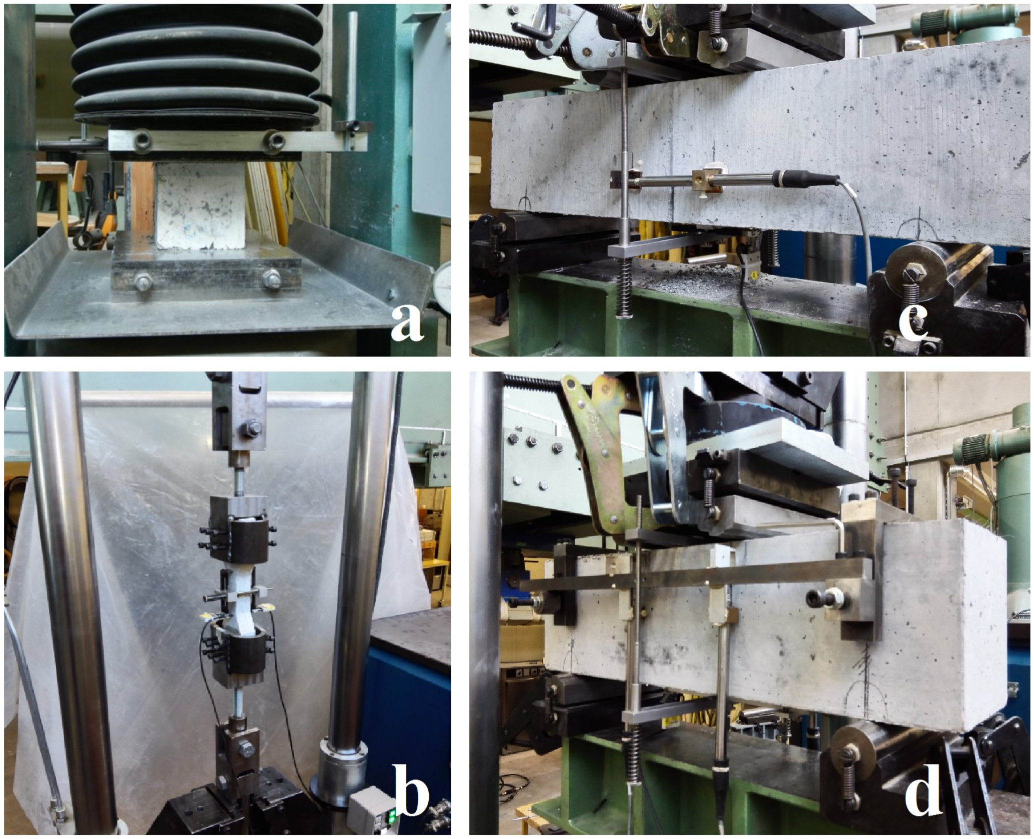

Figure 4: Test machines: a) Machine Perrier type 138-5000 kN used to perform compression tests on cubic specimens; b) Machine Walter Bai type LVF-200 kN used to direct tensile test; c) four-point bending test on notched beams; d) four-point bending test on un-notched beams.

to 0.05 ± 0.01 mm/min according to the guidelines and codes employed for performing the experimental investigation [42, 52, 53]. Carrying out direct tensile tests, the specimens must be loaded along their main axis. This is necessary to prevent that bending occurs. A double hinge mechanism was designed specifically to keep the specimen and the load axis aligned. Furthermore, it is important to avoid any sliding between the machines clamps and the specimens in order to ensure that the entire load is transferred to the specimen. For this purpose an aluminium plate was glued to the specimen's surface as proposed by [53] and a special clamp was designed to have the maximum grip on the aluminium plate as illustrated in Fig. 4(b). When

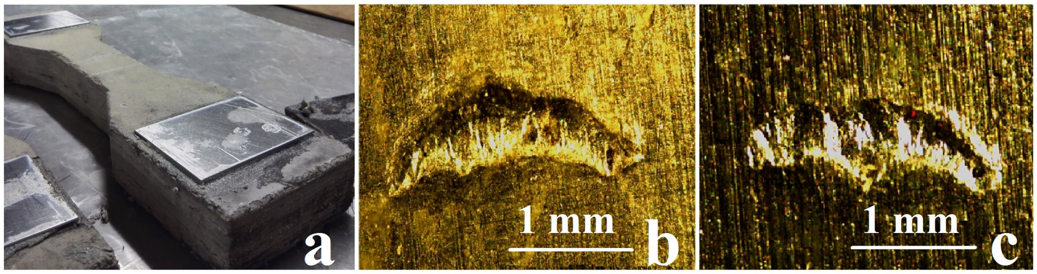

Figure 5: Some pictures related to the direct tensile test: a) Aluminum plate glued on the dog-bone specimen; b) Holes in the aluminum plate before tensile test; c) in the aluminum plate after tensile test.

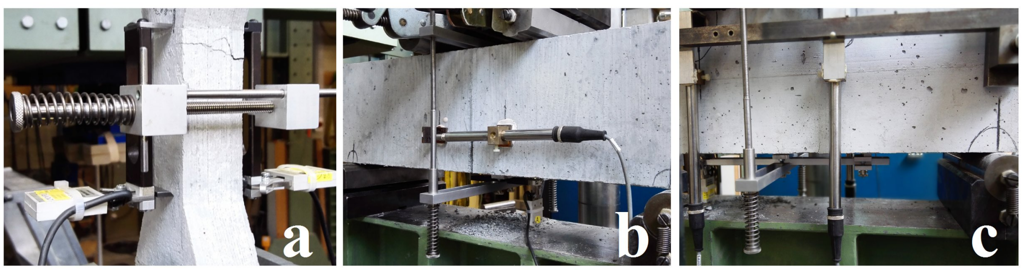

Figure 6: Some pictures related to the extensometers used during the experimental tests: a) The extensometer is placed along the 80 mm characteristic lengths specimen; b) The extensometer is placed at the bottom of the notched beam along 100 mm characteristic length and two LVDT are placed on the sides; c) The extensometer is placed at the bottom of the un-notched beam along 200 mm characteristic length and four LVDT are placed under the rollers loading.

comparing the grooves on the aluminium plate glued on specimens prior and after a direct tensile test (Fig. 5) it can be noted that there are no signs of groove deformation and therefore no sign of slipping. As previously mentioned, the test was carried out by controlling the specimen's axial elongation rate. A high precision extensometer was placed in each side of the specimens. The average of the real time elongations measured by the two sensors permitted to the traction machine to keep the programmed rate of deformation according to [42], see Fig. 6(a).

2.3. Four-point bending flexural test

The machine Walter Bai type LVF-200 kN was used for carrying out the four-point bending flexural tests as well. A standard prismatic specimen is placed on two standard cylindrical supports (see Fig. 4(c)) and loaded through two top rollers placed above the specimen. The distances of the rollers and the supports were compliant with standards [51, 52, 54]. The specimens were sawed in the middle section in order to produce a 45 mm deep v-shaped notch according to [42, 51, 54]. Notched specimens are preferred by norms for the softening materials because the position of the flexural crack is known. The crack opening is measured both in the bottom and in the side of the specimen. Bottom measurement is called Crack Mouth Opening Displacement (CMOD), and side measurement is called Crack Tip Opening Displacement (CTOD). The loading speed is controlled by setting a rate of 0,05 mm/min for the CMOD is imposed until reaching a value of crack opening of 3.5 mm. Sensors used to monitor the CMOD and CTOD are respectively one extensometer and two LVDT displacement transducers with a 100 mm gauge length (Fig. 6(b)). Tests on prismatic un-notched specimen (Fig.4(d)) have been performed as well according to [52]. In these tests the gauge length of the sensor was 200 mm and four LVDTs were used to measure the localized displacement under the top rollers, see Fig. 6(c).

3. Results and discussion

Each test series encompasses several tests. To avoid confusion, a system of samples identification was conceived and is displayed in Table 2 with an example. Three FRC types have been investigated and they are labeled "A", "B" and "C". All of these mortars are commercially available."A" and "C" specimens were cast in four different days and on slightly different environmental conditions."B" specimens were cast in two different days. The samples are shown in Fig. 2.

C. _ . _	type of FRC	A, B, C
_ .2. _	day of casting	1, 2, 3, 4, 5
	beam specimen	1, 2, 3
_ . _ .8	dog-bone specimens	4, 5, 6
	cube specimen	7, 8, 9

Table 2: Specimen identification.

3.0.1. Compressive behavior

Strength was tested on 100 x 100 x 100 mm standardly cured cubes. The peak value, the average value and the coefficient of variation (COV) of the measured compressive stress acting on the sample have been calculated (see Table 3):

$$f_{ci} = \frac{P_i}{A_i}, \qquad f_{Cm} = \frac{\sum_{i=1}^{n} f_{Ci}}{n}, \qquad COV = 100 \cdot \frac{\sigma}{n}, \tag{1}$$

being f_{Ci} the cubic compression in tension of a specimen; P_i the maximum load recorded during the test; A_i the cross section area of the uniformly loaded specimen; R_{cm} the average value of the tension in a campaign of n specimens; σ the standard deviation and n the number of specimens.

The samples of all series shown a similar type of failure. As shown in Fig. 7 the fibers, randomly oriented in the cement matrix, have a higher level of confinement which prevented the classical pyramid failure (usual for plane concrete cubes). It is important to note the beneficial effect of the fibers which avoid the separation of the specimen into separate pieces[4].

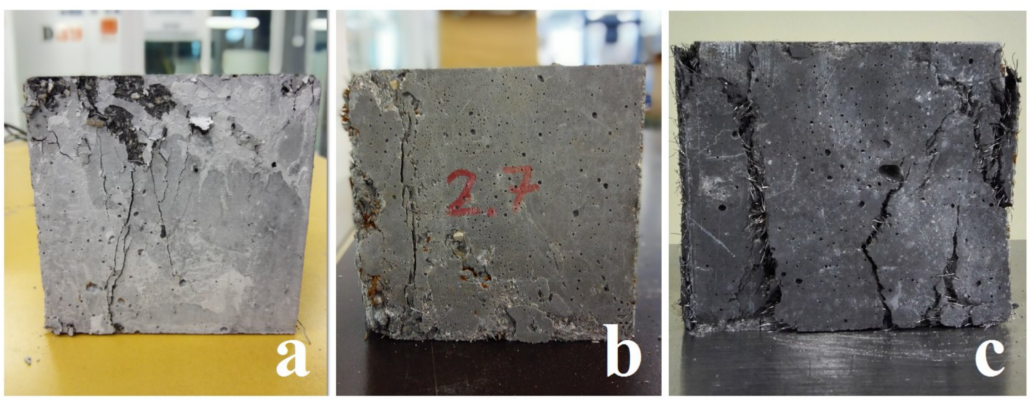

Figure 7: Cracking of samples subjected to the compression test: a) "A" mortar; b) "B" mortar; c) "C" mortar.

[4]Fracture can be modelled, in a nonlinear framework, following [34], whereas recent contributes about damage mechanics can be found in [18, 19, 21]. Bifurcation and stability in the context of homogeneous finite deformations can be found in [35].

3.0.2. Tensile behavior in direct tensile test

Table 3 reports the peak load, the average tension as well as the COV of the cross cracking section of the dog bone specimens. The tensile stress σ_N is obtained by dividing the measured tensile load by the area of the nominal cross section at the crack location (30x40 mm^2, in this case). The total elongation δ (deformation) is obtained by multiplying the axial strain (specific deformation) measured by the characteristic length of the sensors (80 mm). The tensile load-elongation curves $\sigma_N - \delta$, obtained by testing dog-bones specimens, are shown in Fig. 8. It can be observed a series of sudden drops of tensile stress during the load tests in a number of specimens of mortars B and C. These crests and troughs in the stress-strain graphs often occur in SFRC tests and they are caused by one or a combination of the following mechanisms which can be recognized during the crack generation and growth in FRC:

- *Fiber failure*. It is the less common phenomenon and it happens usually in long fibers, where the bond is so high that the fiber can reach rupture.
- *Fiber pull-out*. This is the mechanism that dissipates less energy and it's the most common in straight fibers.
- *Fiber bridging*. Fibers link the two edges of the crack and the stress can be transferred through them. This is the most common phenomenon in non-straight fibers. The energy is absorbed by the deformation of the fiber.
- *Fiber/matrix debonding*. Like the fiber failure, this happens usually in long and well bonded fibers.
- *Matrix crack*. The fiber can contrast the propagation of micro-cracking through the matrix spreading the energy of the crack on a wider surface.

By observing the graphs in Fig. 8 it might be concluded that the crests and troughs affecting the experimental curves about mortars "B" and "C" are linked to the pull-out of the straight fibers used in these SFRCs. The pull-out mechanism was prevented in SFRC "A" by the use of hooked fibers. Dog-bone specimens of "A" SFRC specimens showed also a multi cracking behavior (Fig. 9), probably ascribable to the use of hooked fibers [22]. The hooked part of the fibers tend to prevent the total extraction of the fibers and ensures a higher degree of load redistribution. A multi cracking behavior is

Specimen	f,i (MPa)	f,m (MPa)	COV (%)	Specimen	f,i (MPa)	f,m (MPa)	COV (%)	Specimen	f,i (MPa)	f,m (MPa)	COV (%)
A.1.1	26.51			A.1.4	6.52			A.1.7	88.47		
A.1.2	29.00			A.1.5	5.60			A.1.8	82.75		
A.1.3	30.45			A.1.6	5.79			A.1.9	86.29		
A.2.1	43.68			A.2.4	7.51			A.2.7	81.85		
A.2.2	32.87	34.52	16.25	A.2.5	6.77			A.2.8	92.38		
A.2.3	39.03			A.2.6	6.90	6.30	11.52	A.2.9	95.89	86.42	5.06
A.3.1	30.50			A.3.4	5.42			A.3.7	90.21		
A.3.2	40.54			A.3.5	5.94			A.3.8	83.19		
A.3.3	38.08			A.3.6	6.38			A.3.9	81.41		
A.4.1	26.61			A.4.4	6.15			A.4.7	83.27		
A.4.2	30.67	29.27	6.44	A.4.5	5.20			A.4.8	87.21		
A.4.3	30.54			A.4.6	7.46			A.4.9	84.12		
B.1.1	60.36			B.1.4	10.31			B.1.7	154.25		
B.1.2	58.18			B.1.5	10.44			B.1.8	156.52		
B.1.3	67.63	66.69	9.31	B.1.6	10.02	11.84	15.40	B.1.9	151.32	151.08	2.56
B.2.1	75.92			B.2.4	14.80			B.2.7	151.95		
B.2.2	65.72			B.2.5	11.76			B.2.8	147.24		
B.2.3	72.32			B.2.6	13.73			B.2.9	145.22		
C.1.1	62.08			C.1.4	14.45			C.1.7	148.65		
C.1.2	77.72			C.1.5	11.76			C.1.8	153.98		
C.1.3	65.75			C.1.6	11.28			C.1.9	149.11		
C.2.1	82.16			C.2.4	12.43			C.2.7	144.24		
C.2.2	75.63			C.2.5	11.55			C.2.8	146.58		
C.2.3	82.81	71.52	10.20	C.2.6	14.49	13.06	8.49	C.2.9	140.87	148.61	2.54
C.3.1	77.72			C.3.4	13.85			C.3.7	148.51		
C.3.2	62.53			C.3.5	13.80			C.3.8	153.53		
C.3.3	63.83			C.3.6	13.67			C.3.9	149.04		
C.4.1	71.50			C.4.4	13.80			C.4.7	147.08		
C.4.2	71.47			C.4.5	13.58			C.4.8	147.58		
C.4.3	65.05			C.4.6	12.11			C.4.9	154.16		

Table 3: Results.

always desirable in concrete since it indicates an augmented ductility of the specimen under tension and bending. It is also well-known that an improved ductility and a multi cracking behavior are necessary to have high rotational capacity and good stress redistribution in certain structural elements. Direct tensile tests carried out on dog-bones specimens are initially characterized by an elastic phase. In this phase the contribution of the fibers could not be decoupled, since the matrix characteristics are governing the behavior of the SFRC. Instead, the post-peak phase was strongly influenced by the contribution of the fibers. After the appearance of the first crack, located in the central area of the specimen in B and C series and diffused along the mid-length of the specimen in the series A (Fig. 9), the matrix does not contribute any longer to the resistance. The stresses are transferred completely from the matrix to the (activated) fibers and from the activated fibers to the matrix thanks to the interfacial bond strength. The fibers, bridging the cracks, transfer a part of the load in areas of the specimens that are not yet cracked. Thanks to their slow pull-out resistance and their high ductility, during the growth of the crack opening, a considerable amount of energy is dissipated. This energy dissipation is highlighted by the length of the post-peak curve as well as by the large areas under the graphs (see Fig. 8).

3.1. Tensile behavior by four-point bending flexural test

It is common practice to evaluate the tensile strength of concrete by means of flexural tests. Although well established, this type of test has some limitation when it comes to define the real tensile strength of materials such as SFRC. In this study the flexural strength was evaluated by tensile and flexural tests and a correlation between the two was established by means of the "Composite Material Theory". Table 3 shows the peak load, the average and the COV of the flexural tests. These values and in particular the nominal tension stress σ_N were determined assuming that all the materials remained in the elastic field until failure [42]. The test campaign of SFRC "A" included both notched and un-notched specimens: The tests series A.4 was carried out on un-notched specimens. Most of the tests in all series were carried-out on notched specimens (see Table 3). Results of flexural tests on notched specimens are shown in Fig. 10. Fig. 10 presents the nominal tension-CTOD ($\sigma_N - w$) curves of notched prismatic specimens.

A comparison between notched and un-notched prisms of the test series A.4 permitted to highlight that the un-notched specimens had a multi-cracking behavior (although not pronounced) while notched specimens presented a single crack localized in the middle-span (Fig. 11).

Even though the notched specimens did not show a multi-cracking behavior, the great contribution of the fibers to the ductility was evident. The contribution of fibers to the ductility is easier to be observed in bending rather than in direct tensile test since the flexural test promote the formation of a plastic region in the neighborhood of the middlespan, thus permitting to the specimen important rotations. This plastic behavior is obtained only if the fiber volume exceeds the critical value $V_{f,crit}$. The critical volume of the fibers varies with the matrix and fibers characteristics.

3.1.1. The composite material theory applied to SFRC

According to the Composite Material Theory (CMT), the critical volume of fibers that might promote a strain-hardening behavior can be obtained

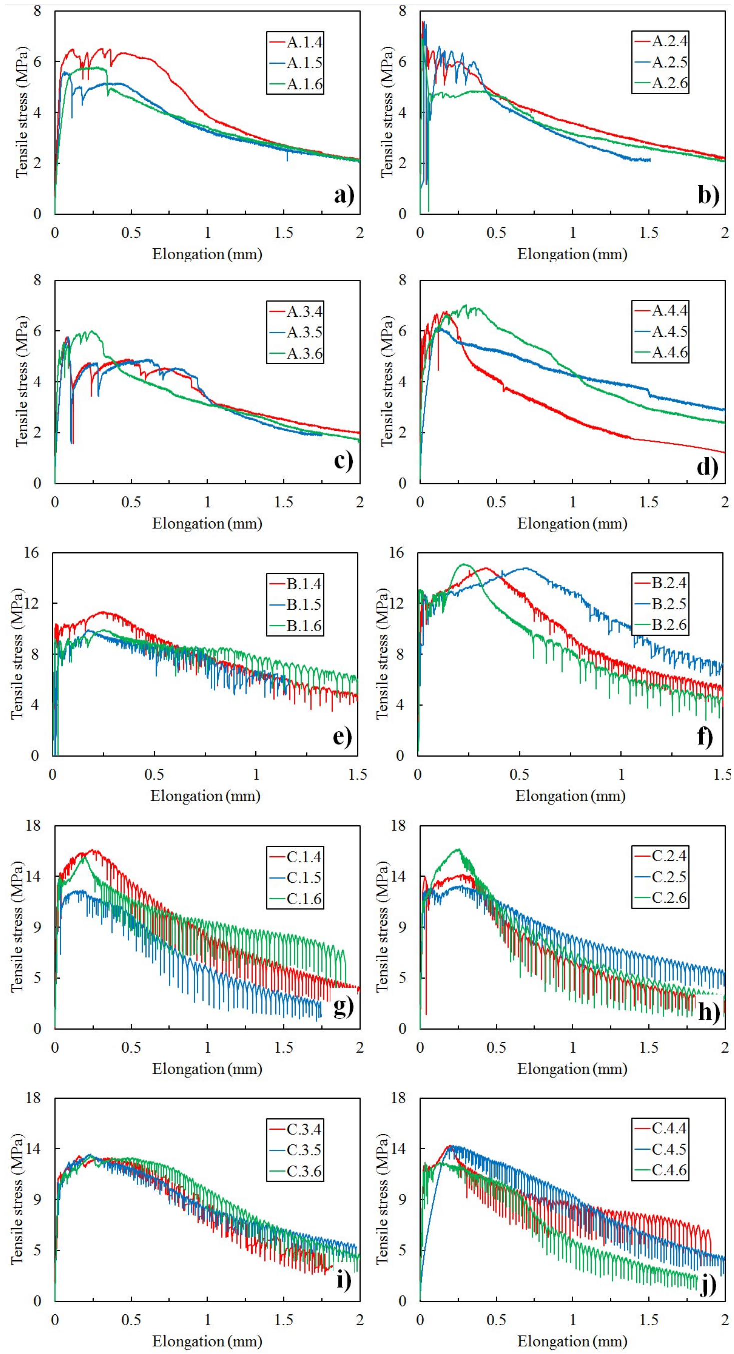

Figure 8: Tensile tension-elongation curves from direct tensile test on the dog-bone specimen series.

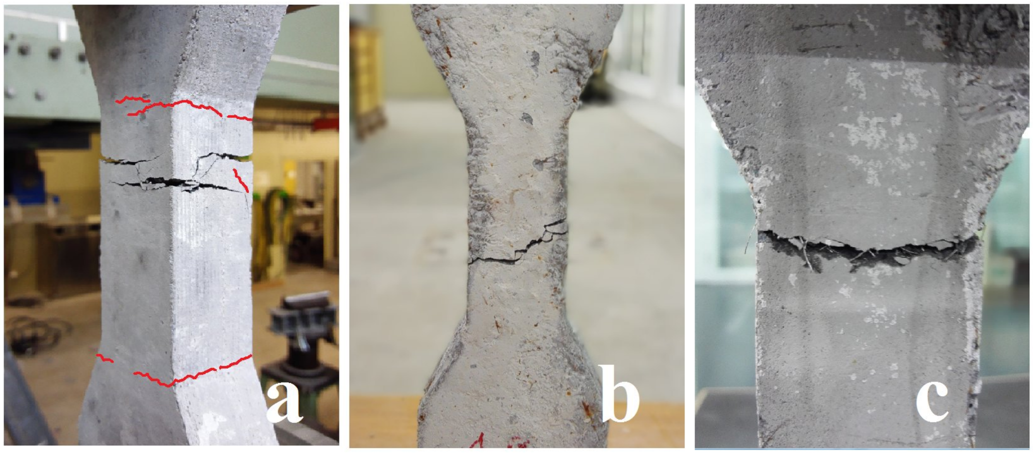

Figure 9: Tensile cracking: a) “A” mortar; b) “B” mortar; c) “C” mortar.

computationally by equating the normal stress acting on the composite σ_c before and after cracking. Before cracking the normal stress acting on the composite is

$$\sigma_c = V_{f,crit} E_f \left(1 - V_{f,crit}\right) \sigma_{mu} \tag{2}$$

whereas after the specimen cracks, the matrix does not contribute any longer to sustain the load and stresses are transferred to the active fibers crossing the cracked section. Then, in this case the tension of the composite becomes

$$\sigma_c = V_{f,crit}\, \sigma_{fu}. \tag{3}$$

By equating (2) and (3) the critical fiber volume that promotes a hardening behavior under direct tensile stress is obtained

$$V_{f,Cr} = \frac{\sigma_{mu}}{\sigma_{fu} - E_f \epsilon_{mu}}, \tag{4}$$

where σ_{mu} is the maximum matrix tension just before the cracking; ϵ_{mu} is the corresponding deformation which, according to the assumption of perfect adhesion, is the same for steel fibers; σ_{fu} is the failure tension of the fibers (rupture or pull-out); E_f is the elastic modulus of the steel fibers.

If the volume of the fibers in the composite exceeds the critical threshold $V_{f,crit}$, a hardening post-peak behavior will be expected. If the volume of fibers is below the critical threshold, then a softening post-peak behavior will be observed. In order to calculate the critical volume of fibers $V_{f,crit}$,

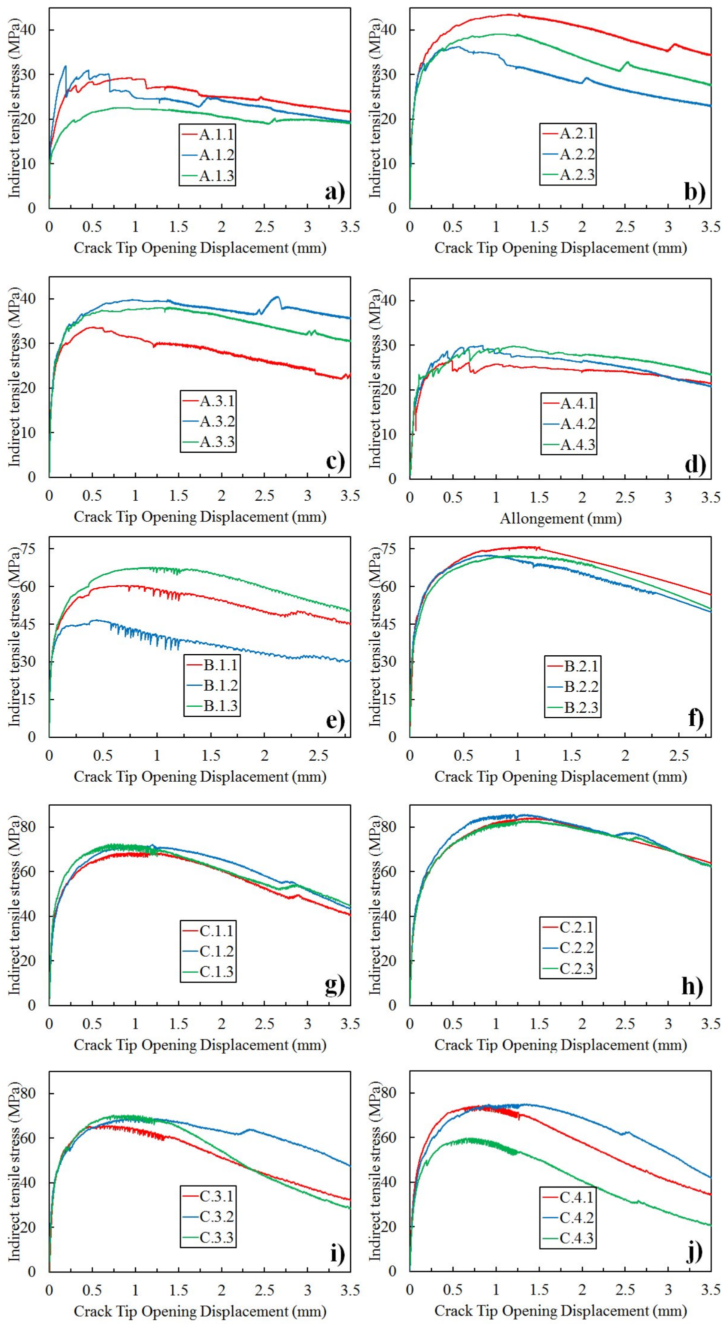

Figure 10: Tension-CTOD by flexion curves from four-point bending flexural test on prismatic specimens.

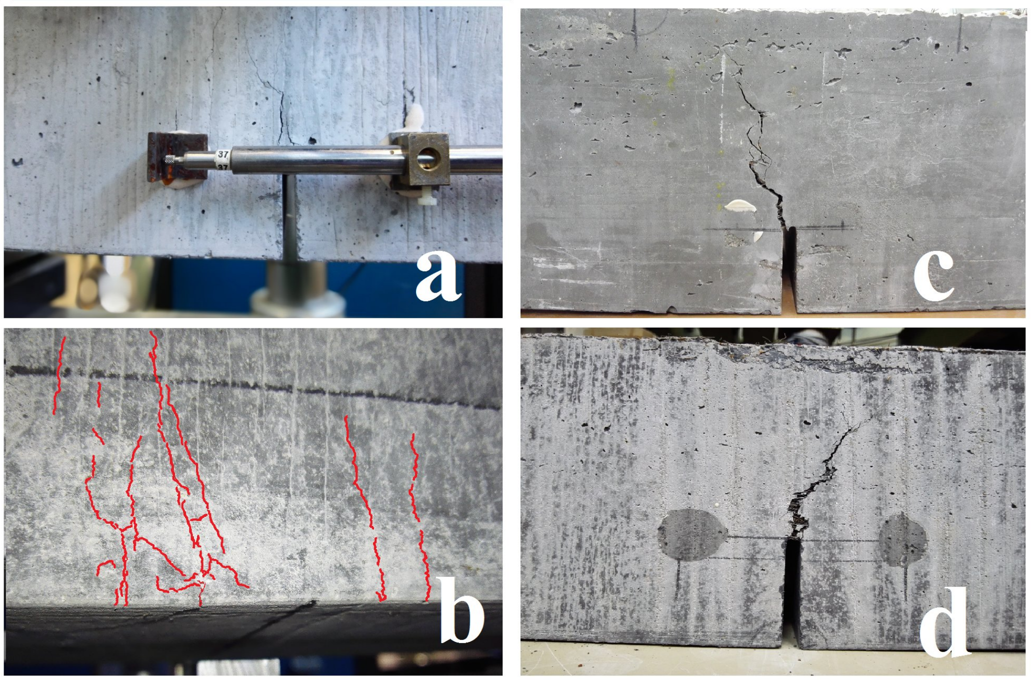

Figure 11: Failure modes observed during the loading bending tests: a) Mono-cracking behavior of notched beam A; b) multi-cracking behavior of un-notched beam A; c) mono-cracking behavior of notched beam B; d) mono-cracking behavior of notched beam C.

it is firstly necessary to model the stress distribution in the cross-section. The pre-peak stress distribution in the cross section can be modeled as in Fig. 12(a) with the tension stresses σ_{mu} and σ_{comp} having the same value. The post peak behavior can be modeled as in Fig. 12(b), where σ_{cu} is the ultimate strength of the composite reached in post-cracking phase. If the neutral axis depth is defined to be equal to $H/4$; the two ultimate bending moments (pre-peak $M_{R,a}$ and post-peak $M_{R,b}$) can be expressed as follows:

$$M_{R,a} = \frac{\sigma_{mu} B H^2}{6}, \qquad M_{R,b} = \frac{\sigma_{cu} B H^2}{32}, \tag{5}$$

where H and B are the dimensions of the cross section.

By equating the moments it follows:

$$\sigma_{cu} = 0.41\sigma_{mu} \leftrightarrow \sigma_{mu} = 2.44\sigma_{cu}, \tag{6}$$

and

$$M_{R,b} \geq M_{R,a} \leftrightarrow \sigma_{cu} \geq 0.41\sigma_{mu}. \tag{7}$$

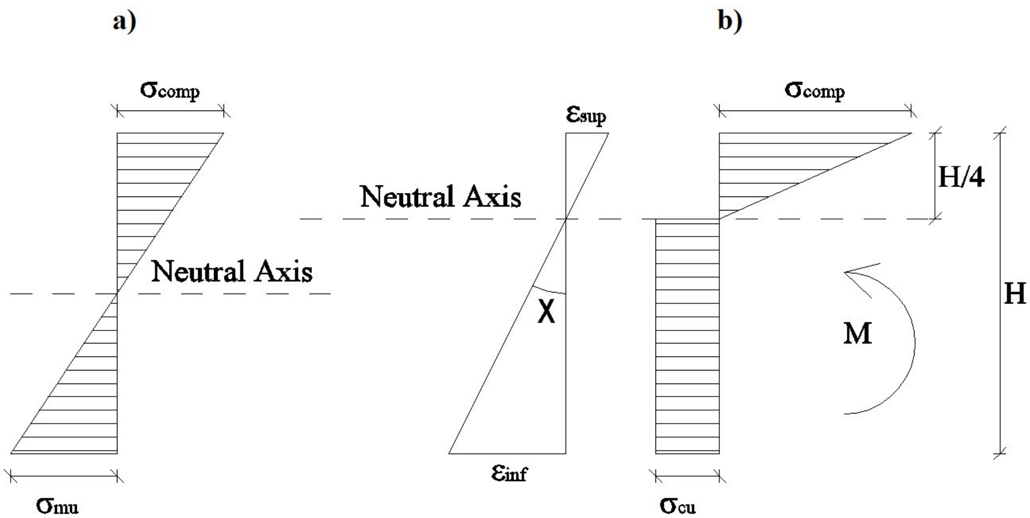

Figure 12: Stress and strain distributions on the cross section of a bent beam: a) Stress distribution before the matrix cracking; b) stress distribution in a post-cracking phase.

The fibers volume that is the boundary between hardening and softening behavior in flexion can be obtained by inserting (6) into (3)

$$V_{f,crit,flexion} = 0.41 \ \frac{\sigma_{mu}}{\sigma_{fu}} \cong 0.41 \ V_{f,crit,traction}. \tag{8}$$

Eq. (8) proves that the hardening behavior in bending stress is also obtained reducing the volume of fibers request to obtain the hardening behavior under tensile load. Fig. 13(a) shows the tensile stress-strain curve obtained by applying (2) and (3) under the hypothesis that the volume of the fibers is equal to $V_{f,crit,traction}$. Fig. 13(b) shows the tensile stress-strain curve obtained by applying (5)a and (5)b under the hypothesis that the volume of the fibers is equal to $V_{f,crit,traction}$. Fig. 13(a) shows that, under pure tension, a post peak plastic plateau will appear, since the volume of fibers is the critical volume. Fig. 13(b) shows a hardening behavior post cracking and maximum tension strength equal to 2.44 times the peak obtained in direct traction. Fig. 14(a) shows the tensile stress-strain curve obtained by applying (2) and (3) under the hypothesis that the volume of the fibers is equal to $V_{f,crit,flexion}$. Fig. 14(b) shows the tensile stress-strain curve obtained by applying (5)a and (5)b under the hypothesis that the volume of the fibers is equal to $V_{f,crit,flexion}$. In this case a softening behavior is seen under pure tensile stresses with the stress decreasing to 0.41 the max stress. A plastic

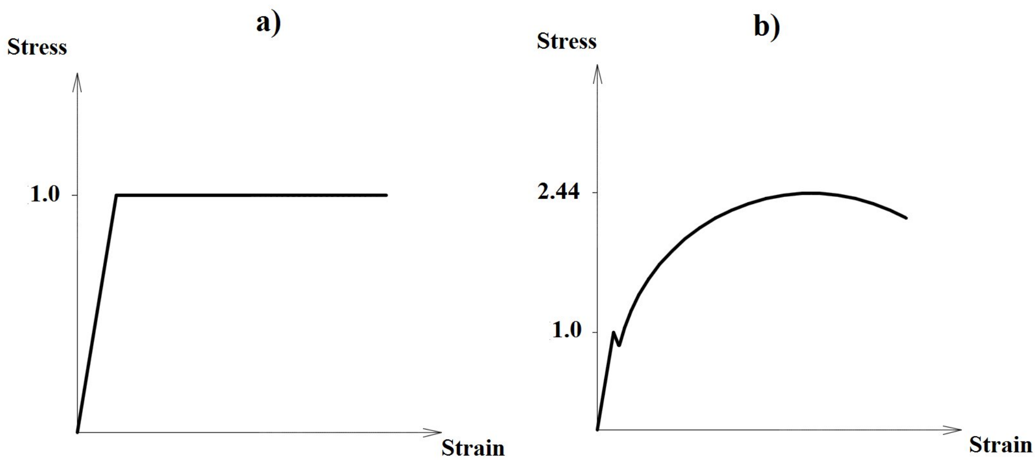

Figure 13: a) Direct tensile curve; b) indirect tensile curve by flexion test with a volume of fibers equal to $V_{f,crit,traction}$.

plateau is observed under bending (Fig. 14(b)). This simple application of the Composite Material Theory (CMT) is sufficient to explain how the tensile strength obtained by flexural tests is always higher than the value obtained in direct tensile tests. The CMT, due its simplicity might be misleading since many assumptions are made. Nevertheless the CMT builds a link between flexural and tensile strength of a SFRC that might prove useful is carefully verified for a specific commercial SFRC. Fig. 15 shows the direct tensile and flexural stress-strain curves obtained by testing specimens in tension and in bending. The similarity of diagram of Fig. 14 and Fig. 15 is evident.

3.1.2. Tensile stress-strain models under bending and direct tensile load

According to the standard used in this study [52], a bilinear tensile stress-strain model can be derived from test data based on three parameters: The tensile strength at the end of the elastic phase, the corresponding strain and the tensile strength at the end of the softening branch. Fig. 16 shows the test data (dog bones) and the curve obtained by the bilinear model derived according to the standard. On SFRC A model, due to the high COV, first and ultimate tensile strength values have been penalized more than 50%. In SFRC B model the reduction of 52% for the first and 37% for the last tensile strength values was caused by a COV of 16% and 8%, while in SFRC C a 37% and 52% of reduction is due to COV of 9% and 18%. The different COVs and behavior of the three SFRCs can be explained by a number of

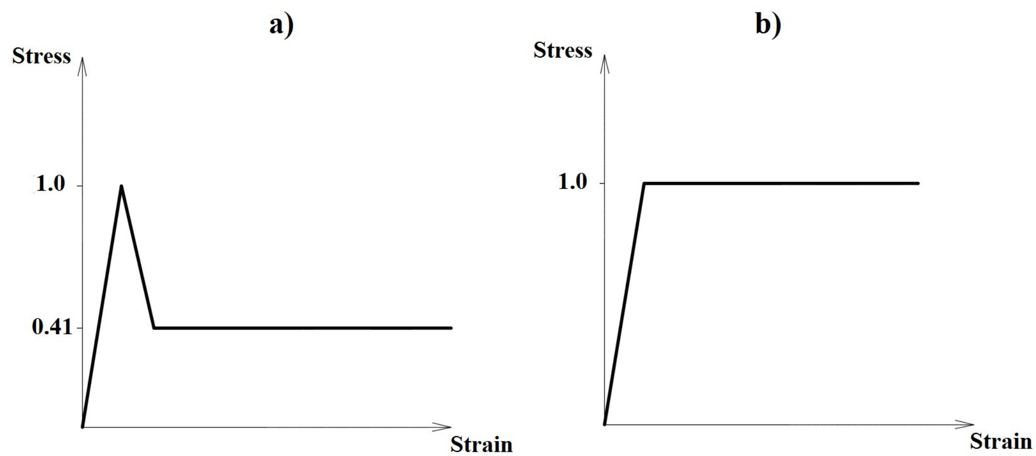

Figure 14: a) Direct tensile curve; b) indirect tensile curve by flexion test with a volume of fibers equal to $V_{f,crit,flexion}$.

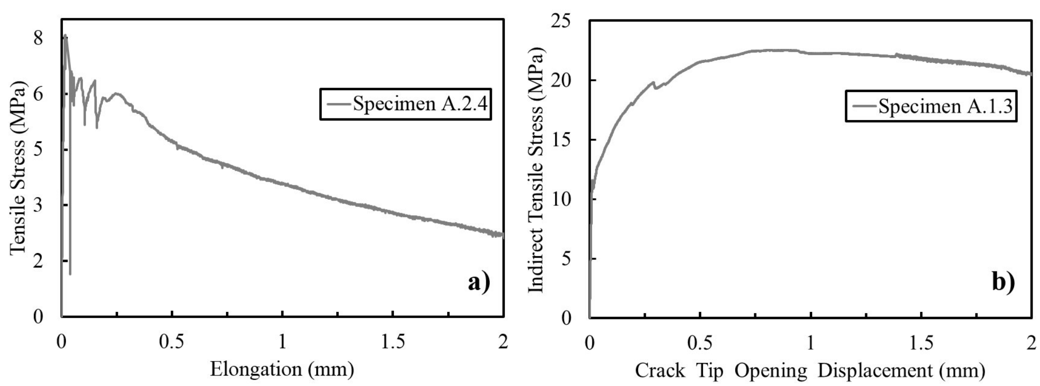

Figure 15: Experimental curves: a) direct tensile test on the specimen A.2.4; b) indirect tensile test provided by bending test on the specimen A.1.3.

factors. The most important ones, according to [55], are the fibers dosage, the geometry of the tested specimen (thickness, in particular), aggregate, fiber size and fiber orientation. Fiber dosage is one of the most important factors of COV variation since a higher dosage of fibers should promote a more even distribution of fiber [11]. As shown in Table 1 the fibres dosage in SFRCs is 1.7%, 2.5% and 3.8% for mortars A, B and C respectively. In fact the COV related to mortar A is slightly larger than that concering mortar C. Fiber dosage seems to be less significant for indirect tensile strength for which the COV was about 20% for all notched specimens of A, B and C

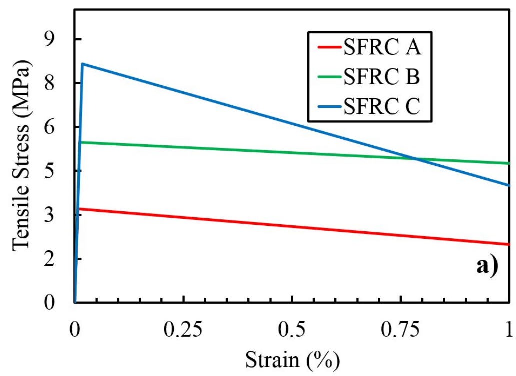

Figure 16: Standard bilinear tensile model.

mortars [25]. The COV in un-notched beams (SFRC A) is less than 6%. The ductility indexes and the tensile strength class, that serves to compare and choose between different commercial SFRCs, can be assessed according to [54]. These indexes are obtained from the models derived by the method proposed by the same standard. Table 4 shows the classification according to ductility and tensile strength standard indexes [54]. Data obtained by testing can be used to construct bilinear tensile constitutive law based on regression analysis. This model was developed for each SFRC and is shown in Fig. 17. Using this bilinear constitutive law, the CMT presented in section 3.3 and the parabola-rectangle compression law according to [56] an indirect tensile stress-strain model was derived for each SFRC. Fig. 18 shows a comparison of the experimental (bending) indirect tensile stress - CTOD results with the results of the analytic model for each concrete. Test results and predictions obtained with the CMT significantly agree.

Class	F2.0	F2.5	F3.0	F3.7	F4.5	F5.5	F6.5	F7.7	F9.0
$f_{1lk,min}$ (Mpa)	2	2.5	3	3.7	4.5	5.5	6.5	7.7	9
Index of ductility		Softening			Plastic			Hardening	
	D_{S0}	D_{S1}	D_{S2}		D_P		D_{H0}	D_{H1}	D_{H2}
$D_{0k,min}$	≤ 0.5	≥ 0.5	≥ 0.7		≥ 0.9		≥ 1.1	≥ 1.3	≥ 1.55
Classification							A	B	C
SFRC							(HPC)	(UHPC)	(UHPC)
Class F							F6.5	>F9.0	F7.7
Class D_0							D_{S1}	D_{S1}	D_{S1}
Class D_1							D_{S0}	D_{S2}	D_{S2}

Table 4: Classification of the SFRCs according to UNI 11039-2:2003.

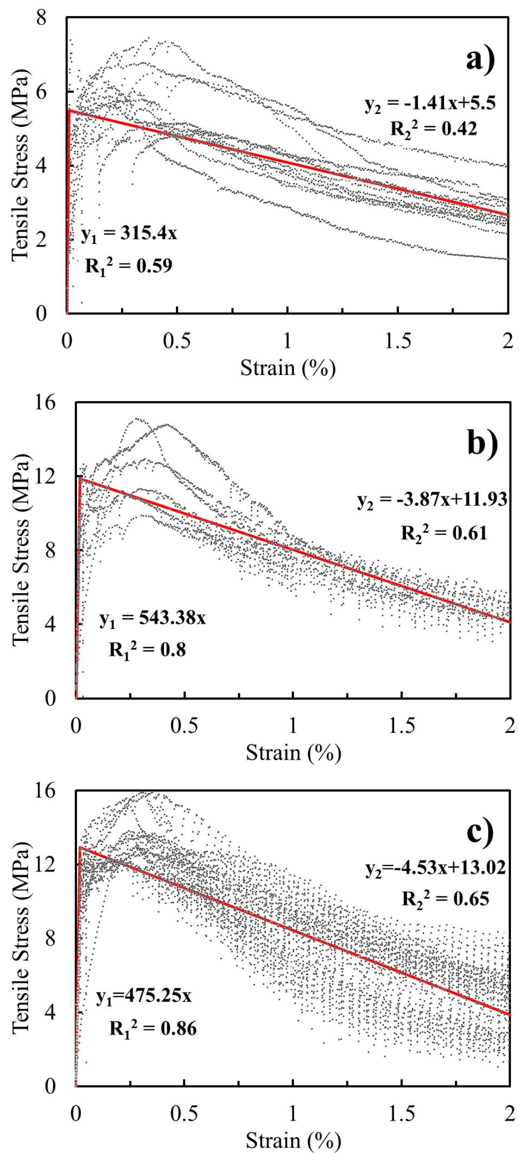

Figure 17: Standard Experimental bilinear tensile model for a) SFRC A; b) SFRC B; c) SFRC C.

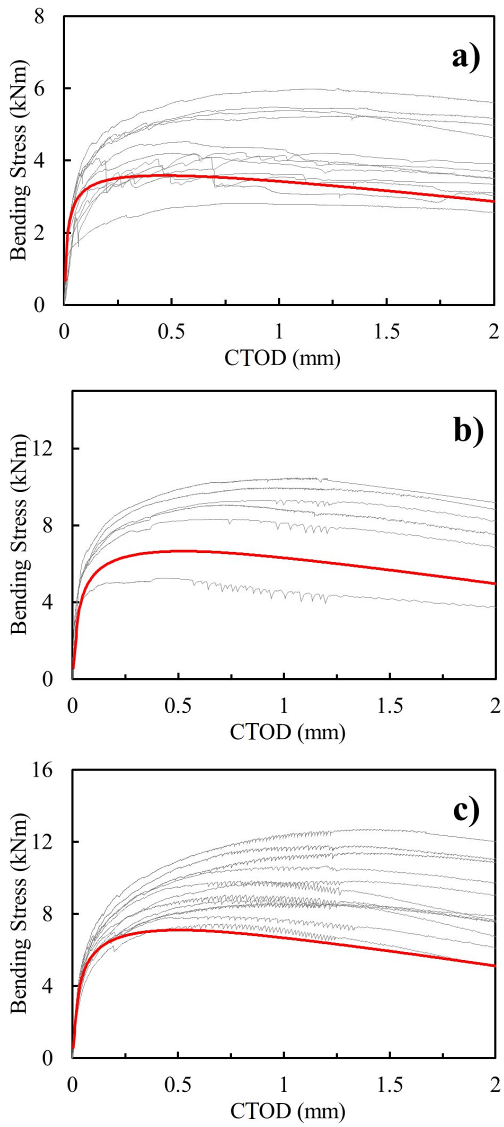

Figure 18: Predictive model Bending Stress-CMOD for a) SFRC A, b) SFRC B, c) SFRC C

4. Conclusion

This paper presents the mechanical characterization of three different SFRCs, two of which are UHPFRCs. The tests have been made according to recent standard protocols for compressive strength, direct tensile strength and flexural strength. The behavior in terms of ductility was assessed according to standards and rated. A tensile constitutive law have been constructed for each concrete and used to predict the indirect tensile stress-strain behavior. Based on the experimental evidence and on the data analyses, the following conclusions can be drawn.
Stress-strain models proposed by codes are sensible to the COV of the tests results. Therefore, a concrete with a greater dispersion of the test results might be rated lower, in term of ductility and strength, that a less performant concrete.
Hooked fibers and higher aspect ratios promote a more ductile behavior and they are proved to be more efficient in providing ductility than a stronger matrix bonding straight fibers w/o higher aspects ratios. This conclusion is drawn on a limited number of tests and therefore must be further confirmed.
All test results obtained with four points bending tests were compared with a model based on the CMT, showing good agreement. The CMT clearly explains the differences of the post-peak behavior of the tests carried out in a four-point bending and under direct tensile stress.
The purpose of the standards used in this study is to supply a fast and inexpensive method for conformity control of a SRFC to be used in field. All tested commercial SFRCs have been classified as low ductility. This might be the effect of the test protocols that might not to be able to fully characterize the stress-strain and ductility characteristics of all SFRC. Nevertheless the principle that it exist a mixture-intensive correlation between the direct and indirect tensile strengths of a SFRC has been found to be true.

Acknowledgments

Authors gratefully acknowledge the financial support provided by HEIG-VD. Financial support from the Italian Ministry of Education, University and Research (MIUR) in the framework of the Project PRIN "COAN 5.50.16.01" (code 2015JW9NJT) is gratefully acknowledged.

Supplementary data

The raw/processed data required to reproduce these findings cannot be shared at this time due to time limitations. However the Authors will provide them soon.

References

[1] Ahlborn TM, Puese EJ, Misson DL. *Ultra-High Performance Concrete for Michigan Bridges*. Material Performance-Phase I 2008:190

[2] Bastien-Masse M, Brühwiler E. *Concrete bridge deck slabs strengthened with UHPFRC*. IABSE Conference Rotterdam Assessment, Upgrading and Refurbishment of Infrastructures 2013;99:236237

[3] Bencardino, F., Condello, A., Ashour, A.F. *Single-lap shear bond tests on Steel Reinforced Geopolymeric Matrix-concrete joints*. Composites Part B, 110, 2017, 62–71.

[4] Caratelli, A., Imperatore, S., Meda, A., Rinaldi, Z. *Punching shear behavior of lightweightfiber reinforced concrete slabs*. Composites Part B, 99, 2016, 257–265.

[5] Conforti, A., Tiberti, G., Plizzari, G.A. *Splitting and crushing failure in FRC elements subjected to a high concentrated load*. Composites Part B, 105, 2016, 82–92.

[6] Choi W.-C., Seok-Joon J., Hyun-Do Y. *Bond and cracking behavior of lap-spliced reinforcing bars embedded in hybrid fiber reinforced strain-hardening cementitious composite (SHCC)*. Composites Part B, 108, 2017, 35–44

[7] Dezi L, Menditto G, Tarantino AM. *Homogeneous structures subjected to successive structural system changes* - ASCE Journal of Engineering Mechanics, 116(8), 1990, 1723-1732.

[8] Dezi L, Tarantino AM. *Time dependent analysis of concrete structures with variable structural system*. ACI Materials Journal, 88(3), 1991, 320-324.

[9] Dezi L, Menditto G, Tarantino AM. *Viscoelastic heterogeneous structures with variable structural system* - ASCE Journal of Engineering Mechanics, 119(2), 1993, pp. 238-250

[10] Eldin HKS, Mohamed HA, Khater M, Ahmed S. *Mechanical Properties of Ultra-High Performance Fiber Reinforced Concrete*. Int J Eng Innov Technol 2014;4:4-10

[11] Finazzi S, Paegle I, Fischer G. & Minelli F. *Influence of bending test configuration on cracking behavior of FRC*. Proceedings of the 3rd All-Russia (International) Conference on Concrete and Reinforced Concrete 2014;3:196-205

[12] Germano, F., Tiberti G., Plizzari, G. *Experimental behavior of SFRC columns under uniaxial and biaxial cyclic loads*. Composites Part B, 85 (2016) 76–92

[13] Gesoglu, M., Gneyisi, E., Muhyaddin, G.F., Asaad, D.S. *Strain hardening ultra-high performancefiber reinforced cementitious composites: Effect offiber type and concentration*. Composites Part B 103, 2016, 74–83

[14] Hannawi, K., Bian, H., Prince-Agbodjan, W., Raghavan, B. *Effect of different types offibers on the microstructure and the mechanical behavior of Ultra-High Performance Fiber-Reinforced Concretes*. Composites Part B 86, 2016, 215–220

[15] Jiang L, Niu DT, Bai M. *Experiment Study on the Frost Resistance of Steel Fiber Reinforced Concrete*. Adv Mater Res 2010;150-151:243-6. doi:10.4028/www.scientific.net/AMR.150-151.243

[16] Lackey T, Desgagne G, Benmokrane B, El-Salakawy E, El-Ragaby A. *Design, Construction and monitoring of four innovative concrete bridge decks using non-corrosive FRP composite bars*. Annu Conf Transp Assoc Canada 2004:1-20

[17] Lanzoni L, Nobili A, Tarantino AM. *Performance evaluation of a polypropylene-based draw-wired fibre for concrete structures*. Construct. Build. Mater. 28 (2012) 798-806.

[18] Lanzoni L, Tarantino AM. *Damaged hyperelastic membranes*. Int. J. NonLinear Mech. 60 (2014) 9-22.

[19] Lanzoni L, Tarantino AM. *Equilibrium configurations and stability of a damaged body under uniaxial tractions*. ZAMP Zeitsc. Angew. Math. Phys. 66(1) (2015) 171-190.

[20] Lanzoni L, Soragni M, Tarantino AM, Viviani M. *Concrete beams stiffened by polymer-based mortar layers: Experimental investigation and modeling*. Construction and Building Materials 105 (2016) 321-335.

[21] Lanzoni L, Tarantino AM. *A simple nonlinear model to simulate the localized necking and neck propagation*. Int. J. NonLinear Mech. 84 (2016) 94-104.

[22] Naaman AE, Najm H. *Bond-slip mechanisms of steel fibers in concrete*. ACI Mater J 1991;88:13545

[23] Nazar S., Ismaiel MA., Ahmed M. *Possibility to Improve Strength and Structural Stability of Bridge Deck Slabs by Using Ultra High Performance Fiber Reinforced Concrete*. IOSR J Mech Civ Eng 2014;11:79-87

[24] Nobili A, Lanzoni L, Tarantino AM. *Experimental investigation and monitoring of a polypropylene-based fiber reinforced concrete road pavement*. Construct. Build. Mater. 47 (2013) 888-895.

[25] Parmentier B, De Grove E, Vandewalle L, Van Rickstal F. *Dispersion of the mechanical properties of FRC investigated by different bending tests*. Tailor Made Concrete Structure Walvraven & Stoelhorst 2008;507512

[26] Popa M, Corbu O, Kiss Z, Zagon R. *Achieving Mixtures of Ultra-High Performance Concrete*. Constructi 2013;1:40-6

[27] Ramli M, Dawood, E. *High-Strength Flowable Mortar Reinforced by Steel Fiber*. Slovak Journal of Civil Engineering 2011;19(3): 10-16

[28] Sanal, I., Ozyurt, N., Hosseini, A. *Characterization of hardened state behavior of self compactingfiberreinforced cementitious composites (SC-FRCC's) with different beam sizes andfiber types*. Composites Part B, 105, (2016) 30–45.

[29] Scott DA, Long WR, Moser RD, Green BH, Daniel JLO, Williams BA. *First International Interactive Symposium on UHPC*. 2016 2016:1-12

[30] Shah, Surendra P, Brandt AM, Ouyang C, Baggot R, Eibl J, Glinicki MA, Krenchel H, Lambrechts A, Li VC, Mobasher B, and Taerwe L. *High performance fibre reinforced cement composites Chapter 6* 2 1996

[31] Simoes, T., Octavio, C., Valena, J., Costa, H., Dias-da-Costa, D., Jlio, E. *Influence of concrete strength and steelfibre geometry on the fibre/matrix interface*. Composites Part B 122 (2017) 156–164

[32] Slater E, Moni M, Alam MS. *Predicting the shear strength of steel fiber reinforced concrete beams*. Constr Build Mater 2012;26:423-36

[33] Stålfibertong, *rekommendationer för konstruction, utförande och provning Betongrapport n.4*. Svenska Betongföreningen 1995

[34] Tarantino AM. *Nonlinear fracture mechanics for an elastic Bell material*. Quart. J. of Mech. and Appl. Math. 50(3), 1997, 435-456.

[35] Tarantino AM. *Homogeneous equilibrium configurations of a hyperelastic compressible cube under equitriaxial dead-load tractions* - Journal of Elasticity, 92, 2008, pp. 227-254.

[36] Vanderwalle L. et al. Recommendation of Rilem TC162-TDF. *Test and design methods for steel fibre reinforced concrete. Design of steel fibre reinforced concrete using the s-w method: principles and applications*. Materials and Structures 2002;35:262-278

[37] Vanderwalle L. et al. Recommendation of Rilem TC162-TDF. *Test and design methods for steel fibre reinforced concrete: sigma-epsilon, Design method (final recommendation)*. Materials and Structures 2003;36:560-567

[38] Yazıcı Ş, İnan G, Tabak V. *Effect of aspect ratio and volume fraction of steel fiber on the mechanical properties of SFRC*. Constr Build Mater 2007;21:12503. doi:10.1016/j.conbuildmat.2006.05.025

[39] Yoo, D.Y., Banthia, N., Yoon, Y.S. *Predicting service deflection of ultra-high-performancefiberreinforced concrete beams reinforced with GFRP bars*. Composites Part B, 99 (2016) 381–397

[40] ACI Committee 544. *ACI 544.4R88* Design consideration for steel Fiber Reinforced Concrete. ACI 544.4R-88America Concrete Institute. ACI Farmington Hills, MI 1996

[41] AFGCSETRA. *Ultra High Performance Fibre-Reinforced Concretes*. Interim Recommendations. AFGC Publication. France 2002

[42] CNR-DT 204. *Guidelines for design, construction and production control of fiber reinforced concrete structures*. National Research Council of Italy 2006

[43] Deutscher Ausschuss für Stahlbeton (DafStb). *Guidelines for steel fiber reinforced concrete*. 23rd draft, richtlinie Stahlfaserbeton, DIN 1045 annex, parts 2007:1-4

[44] ACI Committee 318. *Report ACI 31808/318R-08*. Building code and commentary. Report ACI 318-08/318R-08American Concrete Institute, Farmington Hills, MI, 2008

[45] JSCE. *Recommendations for Design*Recommendations for Design and Construction of High Performance Fiber Reinforced Cement Composites with Multiple Fine Cracks (HPFRCC). Rokug, K. Concrete Engng. Series 2008:82

[46] AENOR UNE 83515. *Hormigones con fibras, Determinación de la resistencia a fisuración, tenacidad y resistencia residual a tracción. Metodo Barcelona*. Asociación Española de Normalización, Madrid, 2010

[47] Fib Model Code for Concrete Structures 2010

[48] Symposium SI, Tecnology C, February S. *CHEMICAL ADMIXTURES TODAY* Mario Collepardi, Enco, Engineering Concrete, Ponzano Veneto (Italy) 2005:527-41

[49] UNI EN 206-1. *Concrete Part 1: Specification, performance, production and conformity* 2006

[50] UNI EN 12390-3. *Testing hardened concrete Compressive strength of test specimens* 2003

[51] UNI 11039-1. *Steel fibre reinforced concrete Definitions, classification and designation* 2003

[52] UNI 11188. *Steel fibres reinforced concrete structural elements Design, execution and control* 2007

[53] PrSIA 2052. *Béton fibré ultra-performant (BFUP)-Matériaux, dimensionnement et exécution* 2015-05

[54] UNI 11039-2. *Steel fibre reinforced concrete Test method for determination of first crack strength and ductility indexes* 2003

[55] Brite-Euram Project BRPRCT980813. *Test and Design methods for Steel Fibre Reinforced Concrete* 2001

[56] EN 1992-1-1. *Design of concrete structures General rules and rules for buildings* 1992

List of Figures

1 Steel fibers used in the mortars: a) Hooked fibers 30/0.35 mm; b) Straight fibers 20/0.3 mm; c) Straight fibers 13/0.175 mm. 4
2 Specimen dimensions. 4
3 a) Compression test on cubic specimen; b) Direct tensile test on dog-bone specimen; c) Four-point bending test on notched beam specimen; d) Four-point bending test on un-notched beam specimen. 5
4 Test machines: a) Machine Perrier type 138-5000 kN used to perform compression tests on cubic specimens; b) Machine Walter Bai type LVF-200 kN used to direct tensile test; c) four-point bending test on notched beams; d) four-point bending test on un-notched beams. 6
5 Some pictures related to the direct tensile test: a) Aluminum plate glued on the dog-bone specimen; b) Holes in the aluminum plate before tensile test; c) in the aluminum plate after tensile test. 7
6 Some pictures related to the extensometers used during the experimental tests: a) The extensometer is placed along the 80 mm characteristic lengths specimen; b) The extensometer is placed at the bottom of the notched beam along 100 mm characteristic length and two LVDT are placed on the sides; c) The extensometer is placed at the bottom of the un-notched beam along 200 mm characteristic length and four LVDT are placed under the rollers loading. 7
7 Cracking of samples subjected to the compression test: a) "A" mortar; b) "B" mortar; c) "C" mortar. 9
8 Tensile tension-elongation curves from direct tensile test on the dog-bone specimen series. 13
9 Tensile cracking: a) "A" mortar; b) "B" mortar; c) "C" mortar. 14
10 Tension-CTOD by flexion curves from four-point bending flexural test on prismatic specimens. 15
11 Failure modes observed during the loading bending tests: a) Mono-cracking behavior of notched beam A; b) multi-cracking behavior of un-notched beam A; c) mono-cracking behavior of notched beam B; d) mono-cracking behavior of notched beam C. 16

12 Stress and strain distributions on the cross section of a bent beam: a) Stress distribution before the matrix cracking; b) stress distribution in a post-cracking phase. 17
13 a) Direct tensile curve; b) indirect tensile curve by flexion test with a volume of fibers equal to $V_{f,crit,traction}$. 18
14 a) Direct tensile curve; b) indirect tensile curve by flexion test with a volume of fibers equal to $V_{f,crit,flexion}$. 19
15 Experimental curves: a) direct tensile test on the specimen A.2.4; b) indirect tensile test provided by bending test on the specimen A.1.3. 19
16 Standard bilinear tensile model. 20
17 Standard Experimental bilinear tensile model for a) SFRC A; b) SFRC B; c) SFRC C. 21
18 Predictive model Bending Stress-CMOD for a) SFRC A, b) SFRC B, c) SFRC C 22